Universal High-Energy Photoelectron Emission from Nanoclusters Beyond the Atomic Limit

Zhou Wang,[1] Abraham Camacho Garibay,[1,2] Hyunwook Park,[1] Ulf Saalmann,[2] Pierre Agostini,[1] Jan M. Rost,[2] and Louis F. DiMauro[1,*]

[1]*Department of Physics, The Ohio State University, Columbus, Ohio, USA*

[2]*Max Planck Institute for the Physics of Complex Systems, Nöthnitzer Straße 38, 01187 Dresden, Germany*

(Received 14 August 2019; revised manuscript received 4 March 2020; accepted 3 April 2020; published 29 April 2020)

Rescattering by electrons on classical trajectories is central to understand photoelectron and high-harmonic emission from isolated atoms or molecules in intense laser pulses. By controlling the cluster size and the quiver amplitude of electrons, we demonstrate how rescattering influences the energy distribution of photoelectrons emitted from noble gas nanoclusters. Our experiments reveal a universal dependence of photoelectron energy distributions on the cluster size when scaled by the field driven electron excursion, establishing a unified rescattering picture for extended systems with the known atomic dynamics as the limit of zero extension. The result is supported by molecular dynamics calculations and rationalized with a one-dimensional classical model.

DOI: 10.1103/PhysRevLett.124.173201

Photoelectron spectroscopy is one of the most versatile and powerful methods to investigate matter. In the well-known photoeffect, weak radiation leads to prompt ionization of an electron with binding energy E_b through absorption of a single photon. This direct emission of photo electrons is also the dominating process if the irradiating laser field is very strong, such that $U_p \gtrsim E_b$, where $U_p = F^2/(4\omega^2)$, which is the average energy of a free electron in the laser field of peak amplitude F and frequency ω. During a laser cycle, the electromagnetic force can be so strong that it drives the electron back to the ion where it rescatters. Such events are rare but can lead to considerable additional energy for the photoelectron of up to $10U_p$. For the electron to reach this characteristic maximal energy requires release and rescattering at specific phases of the oscillating laser field [1–3]. On the other hand, in this so-called above-threshold-ionization (ATI) process the maximal energy is independent of details in the atomic or molecular target electron distributions. This can be understood from the observation that the distributions with an extension of a few atomic units are essentially pointlike compared to the distance of $x_\omega = F/\omega^2$ quantifying the excursion of a free electron in the strong laser field ruling the rescattering process. Remarkably, strong field electron dynamics can be described to a large extent by classical electron trajectories which facilitates the understanding of the process, as well as interpretation and modeling of experimental results.

In the following, we will investigate if and how this rescattering induced photoionization applies to extended targets such as nanoclusters or nanoparticles [4–6] with sizes of the same order of magnitude as x_ω. While previously the production of energetic electrons in extended systems was understood as a thermalization process [7] not linked to strong field rescattering, recent experiments on argon clusters [8] and field-controlled photoemission from dielectric nanospheres [4], as well as theoretical considerations [9] have revealed a characteristic feature of rescattering: the energetic photoelectrons exhibit a strong dependence on the phase of the electromagnetic field. Encouraged by this observation, we will present here a unified rescattering picture valid from atoms to extended systems for high-energy electrons generated in the interaction with an intense laser pulse.

In our work, an intense laser, tunable from near-infrared (NIR, 0.8 μm) to midinfrared (MIR, 1.8 μm) wavelengths, is used to generate a well-defined field driven electronic excursion distance x_ω relative to the target's radius R_{cl}, which is varied by creating clusters from a single up to 10^5 argon atoms. The photoelectron energy distribution (PED) is measured with a time-of-flight spectrometer along the laser polarization. PEDs from nanoclusters are compared with back-to-back measurements from argon monomers under identical laser conditions. The nanocluster size is controlled by the stagnation pressure of the cluster valve and estimated according to the Hagena empirical formula [10–12].

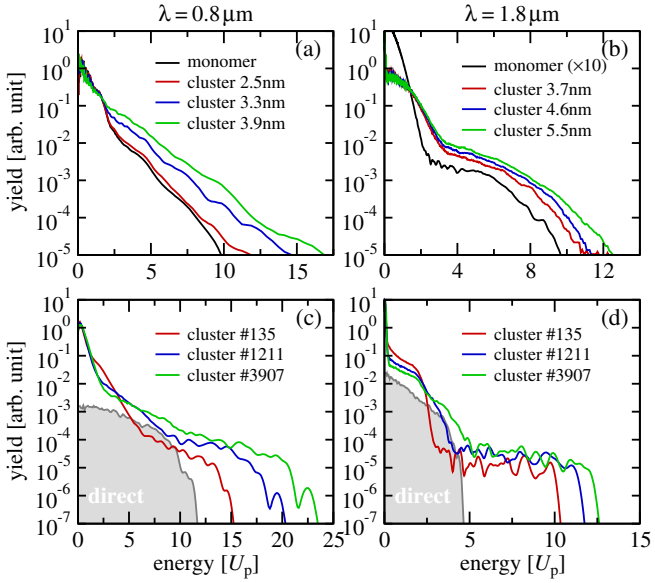

FIG. 1. Photoelectron energy distributions from experiments (a),(b) and MD calculations (c),(d) for the argon atom (black) and different sizes of argon clusters specified in the figures. For clarity, all spectra are normalized to area one. Experimental data are taken at $I = 170$ TW/cm^2 for both 0.8 ($U_p \sim 10$ eV) (a) and 1.8 μm ($U_p \sim 51$ eV) (b), respectively. MD calculations are performed at $I = 600$ TW/cm^2 for both 0.8 ($U_p \sim 36$ eV) (c) and 1.8 μm ($U_p \sim 182$ eV) (d), respectively. The PED spectra shaded in gray and marked "direct" are from calculations with 3907 atoms without hard recollisions of the photoelectrons. The experimental cluster size range is estimated to be $\Delta R \approx \langle R \rangle/3$.

Figures 1(a) and 1(b) provide the measured PEDs for monomers and clusters of different size. The measured PED for monomers (black line) reaches up to $10U_p$, indicative of the maximum energy from rescattering, where an ionized electron is accelerated by the laser field and driven back to collide with the parent ion [18,19]. In contrast, the PEDs from nanoclusters differ from the monomer counterpart, with photoelectron energies increasingly beyond $10U_p$ with growing nanocluster size. At a longer wavelength of 1.8 μm [Fig. 1(b)] the standard rescattering features become more pronounced in the monomer PED showing a break at $2U_p$ and a cutoff at $10U_p$ [3]. The photoelectrons below $2U_p$ result from direct (tunneling) ionization without rescattering, while those in the plateau up to the $10U_p$ limit are from field-driven rescattering. In contrast to the 0.8 μm case, the nanocluster PEDs at 1.8 μm show similar features as the atomic one. The strikingly analogous plateau structure suggests a mechanism rooted in rescattering also for clusters. Similarly as observed for 0.8 μm, the PE spectra at 1.8 μm progressively extends beyond $10U_p$ with the cluster size albeit with a smaller increment, despite the fact that the maximal nanocluster in Fig. 1(b) is larger than in Fig. 1(a).

Early results on the interaction of clusters with infrared laser light were interpreted as stochastic energy absorption through an inverse-Bremsstrahlung process [7]. In this scenario the electrons randomly collide with the ions inside the nanoclusters (and among themselves) and thermalize. Consequently, their energies follow a Maxwell-Boltzmann distribution, which was characterized by a temperature [13,20,21]. Such stochastic energy absorption has no relation to the phase of the laser field, whereas rescattering-dominated dynamics depends sensitively on it. Therefore, we have performed two-color ($\omega, 2\omega$) measurements in order to reveal the phase dependence of the energy absorption in the clusters.

To this end the fundamental driving field (ω) at either NIR (0.8 μm) or MIR (1.7 μm) wavelength is frequency doubled to generate a weak (~3% of ω), phase-locked second harmonic (2ω) field. The beams with temporal and spatial overlap are focused to interact with the targets. The instantaneous total electric field of the synthesized beam can be controlled by the phase delay ϕ between the two fields. Figures 2(a) and 2(b) show the delay-dependent PEDs from argon atoms. As can be seen the atomic cutoff oscillates with ϕ characteristic for rescattering in atoms [22,23] for both fundamental wavelengths. For clusters under identical conditions, as shown in Figs. 2(c) and 2(d) similar oscillations in the high-energy photoelectron yield can be clearly identified with a nearly identical phase dependence. Note that in the two-color measurements, the input energy, average intensity, and pulse duration are kept constant with respect to ϕ. Hence, inverse Bremsstrahlung

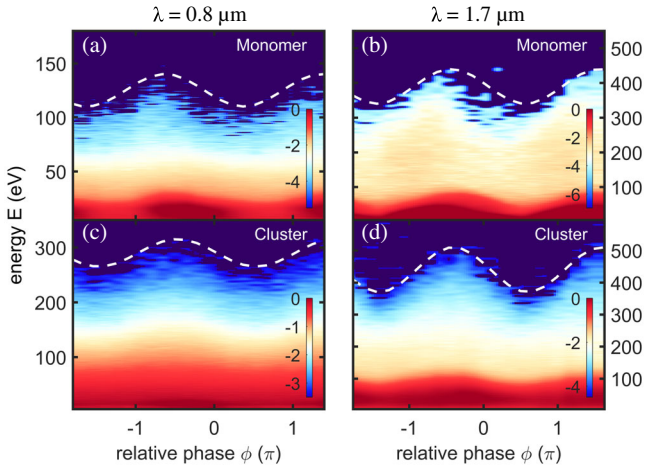

FIG. 2. Two-color ($\omega, 2\omega$) measurement of the photoelectron energy from argon atoms and argon clusters ($R_{cl} \sim 3.2$ nm) at base wavelength 0.8 (corresponding to $\omega_1 = 0.057$ a.u., left panels) and 1.7 μm ($\omega_2 = 0.027$ a.u., right panels). Intensities for each color are $I_{\omega_i} \sim 140$ and $I_{2\omega_i} \sim 5$ TW/cm^2 for $i = 1, 2$. The PEDs are resolved with respect to the delay ϕ between fundamental $\mathcal{E}_\omega$ and the copolarized second harmonic field $\mathcal{E}_{2\omega}$ with $\mathcal{E}_{\text{total}} = \mathcal{E}_{\omega_i} \cos(\omega_i t) + \mathcal{E}_{2\omega_i} \cos(2\omega_i t + \phi)$. White dashed lines are presented as a help to guide the eye.

can be ruled out as an origin of the high-energy cluster photoelectrons. Rather, the almost perfect synchronization between the cutoff modulations in atoms and the corresponding high-energy modulations in clusters point to rescattering as a source for this phenomenon, regardless of the wavelength. This conclusion is consistent with cluster PED measurements using few-cycle MIR pulses [8] and carrier-envelope phase measurements on dielectric nanospheres [4]. We note that many-electron effects in clusters considerably suppress ϕ modulation for low-energy electrons [Figs. 2(c) and 2(d)]. These are attributed to thermalized electrons whose emission occurs at later times when the pulse is no longer present, in contrast to those from atoms [Figs. 2(a) and 2(b)] where such a mechanism is not available.

These PEDs from different cluster sizes at wavelengths 0.8 and 1.8 μm are plotted in Figs. 1(c) and 1(d), respectively. The simulated PEDs, for single-size clusters without focal averaging, exhibit the observed experimental features and trends qualitatively. For both wavelengths, the spectra progressively increase beyond $10U_p$ with growing cluster size, with a larger effect for 0.8 μm than for 1.8 μm, as in the experimental spectra of Figs. 1(a) and 1(b). If hard recollisions are excluded from the simulation as it was done for the black curves enclosing gray-shaded areas in Figs. 1(c) and 1(d), the distributions resemble PEDs familiar from atoms for "direct" electrons, although such electrons can acquire energies beyond $2U_p$, the classical limit for direct electrons in atoms [9], due to the cluster environment. Hence, the simulated PEDs and, in particular, the comparison with the direct processes, also point to recollisions as the source for the high-energy electrons.

In contrast to atoms, rescattering in extended objects such as clusters should depend on the *two* physical spatial scales involved, the nanocluster size described by the cluster radius R_{cl}, and the electron quiver distance x_ω. In a typical strong-field experiment, x_ω is on the order of a few nanometers, which is significantly larger than the extension of the ground-state electron density in an atom or molecule. Consequently, the standard rescattering model assumes that the collision occurs at the atomic origin and—in its simplest version—that the external field rules the electron motion rendering the Coulomb field negligible, especially at high energy. If small, relative to the extension of the quiver distance ($R_{\mathrm{cl}} \ll x_\omega$), the cluster appears in the strong field dynamics as a point scatterer, thus manifesting atomiclike scattering. On the other hand, if the cluster size is comparable to x_ω, as in our experiment in particular for 0.8 μm light ($x_\omega = 1.12$ nm in this case), differences in the recollision dynamics can be expected as electrons may rescatter from any ion or atom in the cluster. This suggests that the electronic energy distribution can be formulated as a function of the dimensionless cluster radius $R = R_{\mathrm{cl}}/x_\omega$, which takes into account our intuition that high-energy photoelectrons from a cluster behave like those of an atom under a strong laser field if the quiver distance of the electron is much larger than the cluster radius.

To establish the high-energy behavior of electrons in clusters it would be desirable to track characteristic electron trajectories in order to reveal their energy gaining process as in the atomic case. At first glance, however, it is impossible to identify a simple mechanism ruling the maximal energy gain in a nanocluster due to its complexity. Yet, it is clear that an energetic backscattered electron is so fast that it will promptly leave the cluster without any further interaction. This means that the vast majority of the electron energy is obtained through a single "last" violent collision while every other previous particle-particle interaction can essentially be neglected. The corresponding trajectory after the "last return" (i. e., an electron being driven back to the cluster by the laser field) can be calculated classically, and seamlessly connects to the three-step model from atoms and molecules [18,19].

To be able to relate cluster rescattering to the original atomic scenario, we have devised a 1D rescattering model which contains the atomic case as a limit (see Supplemental Material [12]). The nanocluster is represented by a square potential with a width of $2R_{\mathrm{cl}}$ and a depth of V. Furthermore, we assume that the cluster gets ionized until the laser field with peak amplitude F is no longer able to remove electrons of the Q-fold charged cluster which retains electrons at the surface with its Coulombic force. This happens if $Q/R_{\mathrm{cl}}^2 = F$ [9,24]. Thus we can replace Q in the potential depth $V = Q/R_{\mathrm{cl}}$ with FR_{cl}^2, which allows us to define a scaled Hamiltonian

$$h(R) = H(R_{\mathrm{cl}}/x_\omega)/U_p. \tag{1}$$

The dynamics driven by $h(R)$ does not depend on the laser parameters (intensity and frequency) explicitly. To determine the photoelectron cutoff in the model, an electron is released from the edge R_{cl} of the cluster at any initial time (or phase ϕ_0 of the laser field, respectively), accelerated by the field, and driven back to scatter at any location x_r within the cluster $|x_r| < R_{\mathrm{cl}}$. The final electron energy $E(\phi_0, x_r; R_{\mathrm{cl}}, x_\omega)$ is maximized numerically with respect to ϕ_0 and x_r which gives the dependence of the scaled cutoff energy on the scaled cluster radius R shown as a gray line in Fig. 3. As one can see, it follows the results from the MD calculations (open symbols) remarkably well, indicating that the dependence on further properties (such as pulse length or energy gain through residual collisions) is weak for the parameters chosen. The open symbols show the photoelectron events with the largest energy from the MD calculations (for details see the Supplemental Material [12]) corresponding to the evolution of the atomic cutoff as a function of cluster size. Thereby the MD results represent calculations for different cluster sizes, photon energies, and pulse intensities underscoring the validity of the scaling.

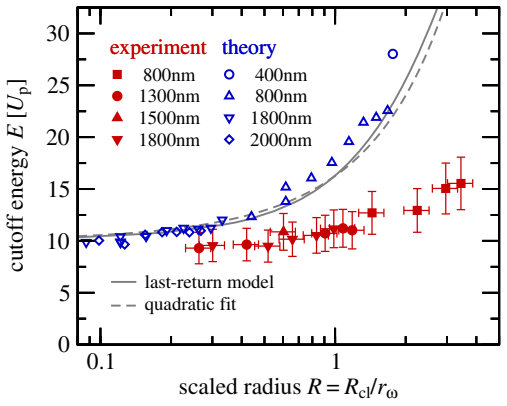

FIG. 3. Evolution of different cutoffs with the scaled cluster radius R. Experimental values (solid symbols) are obtained though the condition $P(E^{\text{cutoff}}) = kP(5U_p)$, with $k = 10^{-3}\ldots10^{-2}$, depending on the wavelength. MD simulation values (open symbols) give the highest energies recorded. The gray-solid line shows the results from the 1D "last return" model (see text), the gray-dashed line is a quadratic fit according to Eq. (2) to it. Data are taken in the range of $I = 150\ldots500$ TW/cm^2, $R_{cl} = 0.9\ldots7.8$ nm, and $T = 45\ldots60$ fs in the experiment and $I = 600$ TW/cm^2, $R_{cl} = 1.0\ldots3.2$ nm, and $T = 60$ fs in the MD calculations.

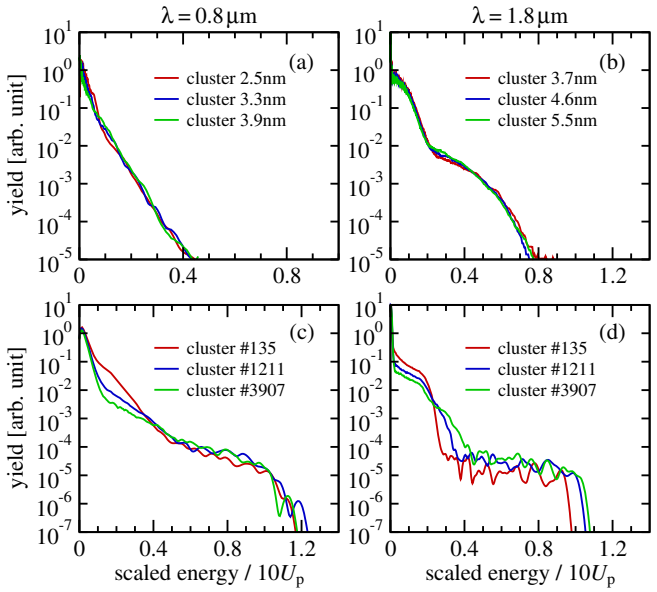

FIG. 4. Photoelectron energy distributions for argon clusters as in Fig. 1 from experiments (a),(b) and MD calculations (c),(d), but with the energy axis rescaled according to the energy scale $E^{\max}(R)$ from Eq. (2).

In the small cluster or long wavelength limit, the electron traverses the entire cluster within a small fraction of an optical cycle and therefore without any significant change in the field phase, and hence the cutoff energy remains around $10U_p$ as in the atomic case for $R = R_{cl}/x_\omega \ll 1$. The depth of the potential plays a minor role for the parameters considered here since the energy for the cutoff is dominated by the drift momentum F/ω. In the large cluster or short wavelength limit, we leave the "atomic regime," and the electron will rescatter from an atom inside the cluster for which the field phase is such that the energy gained from this process is maximized. For increasing R the potential depth V/U_p becomes more important than the drift momentum, since it increases the velocity with which the electron suffers elastic rescattering in the cluster and therefore amplifies the energy gain. Over the energy range covered in Fig. 3 the simple form

$$E^{\max}(R) \approx 10U_p(1 + aR)^2, \tag{2}$$

with $a = 0.275$ (shown as a dashed line in Fig. 3) parametrizes the size-dependent high-energy scale in terms of the theoretical cutoff for our argon clusters very well. We should point out that this fit is only valid over the size range presented here, and that the parameter a has no deeper meaning.

For atoms the $10U_p$ cutoff sets the energy scale for the high-energy part of the PEDs. We see from Eq. (2) that for clusters the scale is amended by the factor $(1 + aR)^2$, depending in a simple way on the scaled cluster radius $R = R_{cl}/x_\omega$. If the high-energy behavior of the rescattered photoelectrons is universal, with the help of the scaled radius R computed from experimental conditions the spectra shown in Fig. 1 should collapse to a single curve when plotted against the scaled photoelectron energy $E/E^{\max}(R)$. In Fig. 4 one can see that this is indeed the case for both the experimental and the theoretical spectra.

In general the maximal energies reached in the experimental spectra are smaller than in the theoretical ones. This is, however, to be expected as the dynamic range of the yield in the experiment is significantly smaller than in the calculations. Yet, reading off values from the experimental spectra close to the noise detection limit by using the condition $P(E^{\text{cutoff}}) = kP(5U_p)$, with k ranging from 10^{-3} to 10^{-2} depending on the wavelength, from the experimental spectra close to the noise detection limit reveals once again the universal high-energy rescattering behavior, see full (red) symbols in Fig. 3. Consistent with the experimentally determined cutoff the rise of the experimental curve with R is weaker than for the theoretical cutoff [black line and open (blue) symbols]. Comparison with the theoretical result suggests that a noise threshold at least reduced by a factor 100 would be necessary to reveal the cluster cutoff. However, the cutoff is only one, albeit well-known, consequence of strong-field rescattering dynamics. As we have demonstrated in this work with the help of size varying clusters, strong field rescattering dynamics is characterized by a universal high-energy behavior of photoelectron distributions over wide range of energies revealed by the R-dependent energy scale function (2). This remarkable property has so far gone unnoticed, since for pointlike systems relative to the quiver motion, such as atoms and molecules, the scale function reduces to the well-known single point, $E^{\max}(0) = 10U_p$.

Finally, to understand qualitatively the limits of this universal behavior, we recall the conditions under which it was demonstrated. The mean-free-path length for the energetic electrons should be large enough to ensure that the photo-electron does not undergo further collisions after the violent one which lead to its decisive energy gain. Furthermore, in contrast, e.g., to the scenario of Ref. [4] the pulse must be long enough such that saturation in the charging is reached in order to have $Q/R_{\mathrm{cl}}^2 = F$, which allows us to formulate the scaled Hamiltonian (1). Last but not least, the scale function (2) will have a more complicated form if the Coulomb potential of the cluster is relevant, which applies to large charging Q. This is, however, beyond the scope of this Letter.

In conclusion, by experiments controlling cluster size and laser parameters of intense pulses interacting with argon clusters, we have revealed that a universal high-energy photoelectron regime exists, which is characterized by hard recollisions of laser driven electrons from ions or atoms in the cluster in analogy to atoms. Universality emerges as the high-energy scale depends only on a combination of cluster size and laser parameters, namely, the ponderomotive energy and the cluster radius scaled by the quiver amplitude $R = R_{\mathrm{cl}}/x_\omega$, verified within the limits of experimental constraints and uncertainties in this experiment. We expect this characteristic length scale to be also relevant for intense light-driven processes in nanostructures or large polyatomic biomolecules.

This material is based upon work supported by the Air Force Office of Scientific Research under MURI Grant No. FA9550-16-1-0013 and by the National Science Foundation under Grant No. PHY-1605042. The DiMauro group acknowledges support from the Ohio Supercomputer Center through Project No. PAS0207.

Z. W. and A. C. G. contributed equally to this work.

*dimauro.6@osu.edu

[1] G. G. Paulus, W. Becker, W. Nicklich, and H. Walther, Rescattering effects in above-threshold ionization: A classical model, J. Phys. B **27**, L703 (1994).
[2] J. Tate, T. Auguste, H. G. Muller, P. Salieres, P. Agostini, and L. F. DiMauro, Scaling of Wave-Packet Dynamics in an Intense Midinfrared Field, Phys. Rev. Lett. **98**, 013901 (2007).
[3] P. Colosimo *et al.*, Scaling strong-field interactions towards the classical limit, Nat. Phys. **4**, 386 (2008).
[4] S. Zherebtsov *et al.*, Controlled near-field enhanced electron acceleration from dielectric nanospheres with intense few-cycle laser fields, Nat. Phys. **7**, 656 (2011).
[5] F. Süßmann *et al.*, Field propagation-induced directionality of carrier-envelope phase-controlled photoemission from nanospheres, Nat. Commun. **6**, 7944 (2015).
[6] M. F. Ciappina *et al.*, Attosecond physics at the nanoscale, Rep. Prog. Phys. **80**, 054401 (2017).
[7] T. Ditmire, T. Donnelly, A. M. Rubenchik, R. W. Falcone, and M. D. Perry, Interaction of intense laser pulses with atomic clusters, Phys. Rev. A **53**, 3379 (1996).
[8] B. Schütte, P. Ye, S. Patchkovskii, D. R. Austin, C. Brahms, C. Strüber, T. Witting, M. Y. Ivanov, J. W. G. Tisch, and J. P. Marangos, Strong-field ionization of clusters using two-cycle pulses at 1.8 μm, Sci. Rep. **6**, 39664 (2016).
[9] U. Saalmann and J. M. Rost, Rescattering for Extended Atomic Systems, Phys. Rev. Lett. **100**, 133006 (2008).
[10] O. F. Hagena, Cluster ion sources (invited), Rev. Sci. Instrum. **63**, 2374 (1992).
[11] F. Dorchies, F. Blasco, T. Caillaud, J. Stevefelt, C. Stenz, A. S. Boldarev, and V. A. Gasilov, Spatial distribution of cluster size and density in supersonic jets as targets for intense laser pulses, Phys. Rev. A **68**, 023201 (2003).
[12] See Supplemental Material at http://link.aps.org/supplemental/10.1103/PhysRevLett.124.173201 for further details and discussion, which contains Refs. [10,13–17].
[13] E. Springate, S. A. Aseyev, S. Zamith, and M. J. J. Vrakking, Electron kinetic energy measurements from laser irradiation of clusters, Phys. Rev. A **68**, 053201 (2003).
[14] Y. L. Shao, T. Ditmire, J. W. G. Tisch, E. Springate, J. P. Marangos, and M. H. R. Hutchinson, Multi-keV Electron Generation in the Interaction of Intense Laser Pulses with Xe Clusters, Phys. Rev. Lett. **77**, 3343 (1996).
[15] U. Even, The Even-Lavie valve as a source for high intensity supersonic beam, EPJ Tech. Instrum. **2**, 17 (2015).
[16] D. W. Schumacher and P. H. Bucksbaum, Phase dependence of intense-field ionization, Phys. Rev. A **54**, 4271 (1996).
[17] S. Alvarez, A cartography of the van der Waals territories, Dalton Trans. **42**, 8617 (2013).
[18] K. J. Schafer, B. Yang, L. F. DiMauro, and K. C. Kulander, Above Threshold Ionization Beyond the High Harmonic Cutoff, Phys. Rev. Lett. **70**, 1599 (1993).
[19] P. B. Corkum, Plasma Perspective on Strong Field Multiphoton Ionization, Phys. Rev. Lett. **71**, 1994 (1993).
[20] V. Kumarappan, M. Krishnamurthy, and D. Mathur, Two-dimensional effects in the hydrodynamic expansion of xenon clusters under intense laser irradiation, Phys. Rev. A **66**, 033203 (2002).
[21] V. Kumarappan, M. Krishnamurthy, and D. Mathur, Asymmetric emission of high-energy electrons in the two-dimensional hydrodynamic expansion of large xenon clusters irradiated by intense laser fields, Phys. Rev. A **67**, 043204 (2003).
[22] D. Ray, Z. Chen, S. De, W. Cao, I. V. Litvinyuk, A. T. Le, C. D. Lin, M. F. Kling, and C. L. Cocke, Momentum spectra of electrons rescattered from rare-gas targets following their extraction by one- and two-color femtosecond laser pulses, Phys. Rev. A **83**, 013410 (2011).
[23] S. Skruszewicz, J. Tiggesbäumker, K.-H. Meiwes-Broer, M. Arbeiter, T. Fennel, and D. Bauer, Two-Color Strong-Field Photoelectron Spectroscopy and the Phase of the Phase, Phys. Rev. Lett. **115**, 043001 (2015).
[24] U. Saalmann, Resonant energy absorption of rare-gas clusters in strong laser pulses, J. Mod. Opt. **53**, 173 (2006).

Supplemental Material

"Universal high-energy photoelectron emission from nanoclusters beyond the atomic limit"

Experimental Setup

In the experiment, the nanoclusters are produced by an Even-Lavie [S1] pulsed valve backed with high-pressure argon gas, ranging from 3 and up to 50 bar, at room temperature. The nanocluster beam is skimmed by a nickel skimmer and delivered into a home-built time-of-flight spectrometer. Nanocluster radii are estimated by the Hagena empirical formula [S2]. MIR ($1.3-2.0\,\mu$m) light is generated by a commercial optical parametrical amplifier (HE-TOPAS, Light Conversion) pumped by a home-built 1 kHz Ti:sapphire amplifier with 60 fs pulse duration. The laser beam is focused into the TOF spectrometer and interacts with the nanoclusters, and the PE signals are collected with a micro-channel-plate detector and converted by a high-speed digitizer (Acqiris U1065A, Keysight Technologies). PE energies are calculated based on its field-free flight time. For direct comparisons with the atomic cases, PE emission from atomic monomers are measured by filling the time-of-flight spectrometer with low-pressure ($\approx 10^{-4}$ Torr) atomic gas, while the laser conditions are kept identical. The laser intensity is estimated by the $2U_p$ break and $10U_p$ cutoff of the PE distribution from atomic monomers.

In the two-color $(\omega, 2\omega)$ measurement, a collinear setup is applied to generate the two-color field. The second harmonic field at 2ω frequency is generated by frequency-doubling the fundamental frequency with a 250-μm-thick BBO crystal. The polarization of the fundamental laser beam is controlled by a half-wave plate centered at ω, and kept parallel to the second harmonic field. The delay between the fundamental and the second harmonic beams is compensated by birefringent A-cut calcite plates and controlled by a wedge pair with sub-laser-cycle precision. The synthesized two-color field, focused by a silver mirror, is spatially clipped by an iris to guarantee a matched Gouy phase across the focus [S3]. The intensity of the two-color beam is estimated by the $2U_p$ break along with its modulation amplitude of the PE distributions from atomic monomers.

Experimental Photo-electron Angular Distribution

Further verification of the field-driven nature of photoelectron emission from clusters (both direct and backscattered) is obtained from the measurement of the angular electron momentum distribution at different wavelengths. Previous works have found photoelectron emission to be anisotropic for the case of clusters subjected to 0.8 μm radiation [S4, S5], as is the case for atomic targets. Here we have measured back-to-back the wavelength-dependent photoelectron emission anisotropy from both monomers and clusters, as shown in Fig. S1. Photoelectron emission is clearly anisotropic for all wavelengths, where the highest energy emission occurs along the laser polarization (i.e. parallel to the abscissa), being anisotropy more dramatic at longer wavelengths. Furthermore, when compared to their atomic counterpart, photoelectron momentum distributions from cluster appears to be less anisotropic.

Anisotropy therefore agrees with the expected behavior from field-driven photoelectrons for both monomers and clusters. Nonetheless, anisotropy from clusters is not as large as the atomic case due to the presence of more scatterers along the electron path which provide with additional transverse momentum. Finally, the evolution of anisotropy with respect to wavelength further reinforce the idea of a scattering mechanism resembling the atomic one at MIR pulses, in accordance to the rescattering hypothesis.

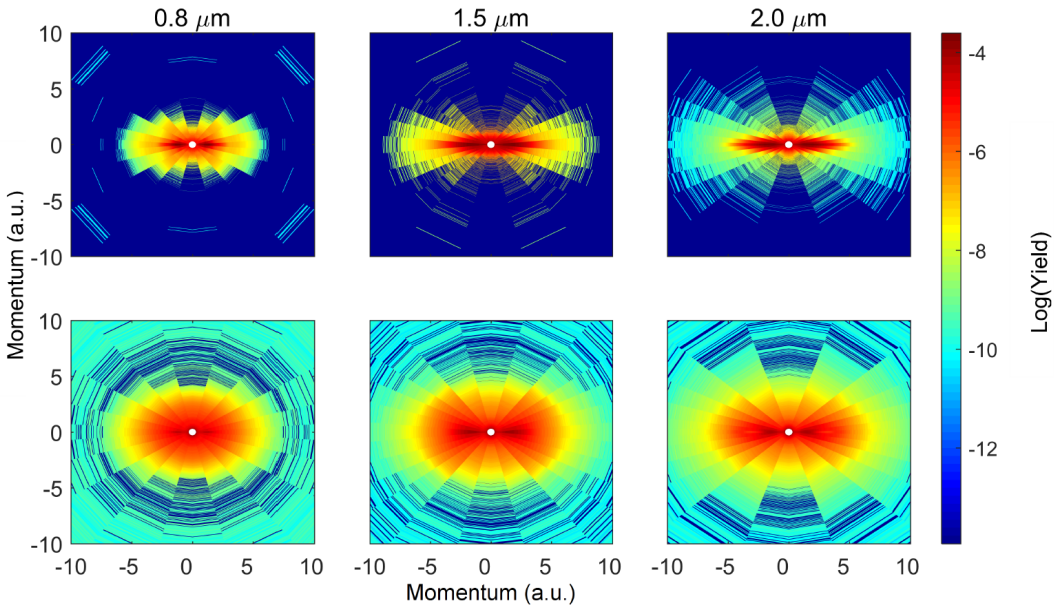

Figure S1: Wavelength-dependent angular photo-electron momentum distribution. Monomers are shown in the upper panels, while the lower panels correspond to emission from clusters. The driving wavelengths are, from left to right: 0.8 μm, 1.5 μm and 2.0 μm. The laser polarization lies along the abscissa, corresponding to the emission of the most energetic electrons.

Theoretical description

MD simulations: In the MD simulations, the nanocluster is constructed inside a sphere of radius $R_{\rm cl}$ following an icosahedral geometry with an interatomic distance of 7.1 au [S6]. A small spatial shift of random orientation and magnitude is applied to each atom (up to 0.5 au) and electron (up to 0.1 au from the atomic center) at the beginning of every realization.

The electrons and ions are considered as classical particles and propagated according to Newtons equations of motion. The interaction between the electron i and ion j with charge q_j are treated with a soft-core Coulomb potential

$$W_{ij}(\mathbf{r}_i, \mathbf{R}_j) = \frac{q_j}{\sqrt{|\mathbf{r}_i - \mathbf{R}_j|^2 + \alpha^2}},$$

(with $\alpha = 1/I_p$, $I_p = 0.579$ au for Argon) except for the following case. If an electron i enters a region close to an ion j with their distance $r_{ij} < r_{\rm Sc}$ ($r_{\rm Sc} \sim 1.73$ au, defines a region where the interaction is assumed to be binary) and the electrons kinetic energy is larger than the binding energy, it propagates along an collisional analytical trajectory following the Keplers law. Such a scheme incorporates the hard collisions to produce the high- energy electrons, which is absent in the soft-core potential alone.

A slightly higher intensity is used in the MD simulations as compared to the experiment since ionization in the simulations is purely classical, which requires higher field strength to field ionize an atom over the barrier. Whenever an electron escapes the vicinity of its parent ion ($r > r_{\rm VdW}$, the Van der Waals radius $r_{\rm VdW} \approx 3.55$ au), the charge state is increased by one and another electron is initialized at the bottom of the soft-core potential. This reflects the increasing ionization potential for ions with higher charge states, while at the same time allowing for a faster computation at early stages in the simulation.

Focal Averaging Effects: Experimental measurements cannot be exempted from focal effects originating from the varying intensity inside the interaction volume. This translates to clusters located along this profile experiencing different values of the ponderomotive energy U and field-driven excursion r_ω, each varying in a different manner with respect to intensity I, namely $U \propto I$ and $r_\omega \propto I^{1/2}$. Assuming a Gaussian beam profile with cylindrical symmetry, focal averaged spectra are obtained by averaging over the radial distance ρ in the focal volume, whereby

$$I(\rho)/I(0) = U(\rho)/U(0) = \exp(-\rho^2), \tag{S1}$$

with $I(0)$ and $U(0)$ being intensity and ponderomotive energy on the beams axis, in the main text simply referred to as I and U_p, respectively. With N_ρ the amount of electrons being released from a cluster located at ρ and $P_\rho(E)$ being the corresponding (normalized) spectrum, the focal-averaged spectrum is given by

$$P(E) = \frac{\int_0^\infty \mathrm{d}\rho\, \rho\, N_\rho P_\rho(E)}{\int_0^\infty \mathrm{d}\rho\, \rho\, N_\rho}. \tag{S2}$$

For the sake of simplicity we assume that the spectra across the focus only scale with respect to U, while r_ω and R_cl remain constant. Hence, spectra along the focus are simply scaled versions of the one at the beam axis, referred to as $P_*(E)$ below. Thus, our proposed simple scaling of the intensity-dependent spectra allows, by means of the parameter $\varepsilon = E/U(\rho)$, to write

$$P_\rho(E) \equiv P_*(\varepsilon)\frac{d\varepsilon}{dE} = \frac{1}{U(\rho)} P_*\big(E/U(\rho)\big). \tag{S3}$$

If one, furthermore, assumes that the emitted electron yield scales linearly with intensity $N_\rho = N_0\, I(\rho)/I(0)$, one arrives at

$$P(E) = \frac{1}{U_\mathrm{p}} \int_0^1 \frac{\mathrm{d}U}{U} P_*(E/U)\,, \tag{S4}$$

whereby $\mathrm{d}U/U = -2\rho\,\mathrm{d}\rho$ was used, which follows from (S1). This procedure clearly fails at the low-energy side of the spectrum, but is a sensible approach for high-energy electrons and for the cutoff in particular. Examples of the resulting spectra obtained with this procedure are seen in Fig. S2. As is also observed in the experiment for both atoms and clusters, the plateau displayed at the peak intensity gets ultimately being measured as a hump due to this effect.

"Last return" model: Resembling the three-step atomic rescattering, we trace the last return electron in a nanocluster by strong field dynamics in a box potential. Assuming a laser pulse of constant intensity, the essential electronic dynamics to reach the highest final energies can be described as a 1-dimensional system with Hamiltonian

$$H = \frac{1}{2}[p - A(t)]^2 + V(x)$$

where $A(t)$ is the vector potential of the laser field and the potential

$$V(x) = \begin{cases} -V_\mathrm{cl} & \text{for } |x| \le R_\mathrm{cl} \\ 0 & \text{for } |x| > R_\mathrm{cl} \end{cases}$$

is a simple box potential representing the ionic background of the nanocluster. Hence, the cluster potential is characterized by two parameters, its width $2R_\mathrm{cl}$ and its depth V_cl.

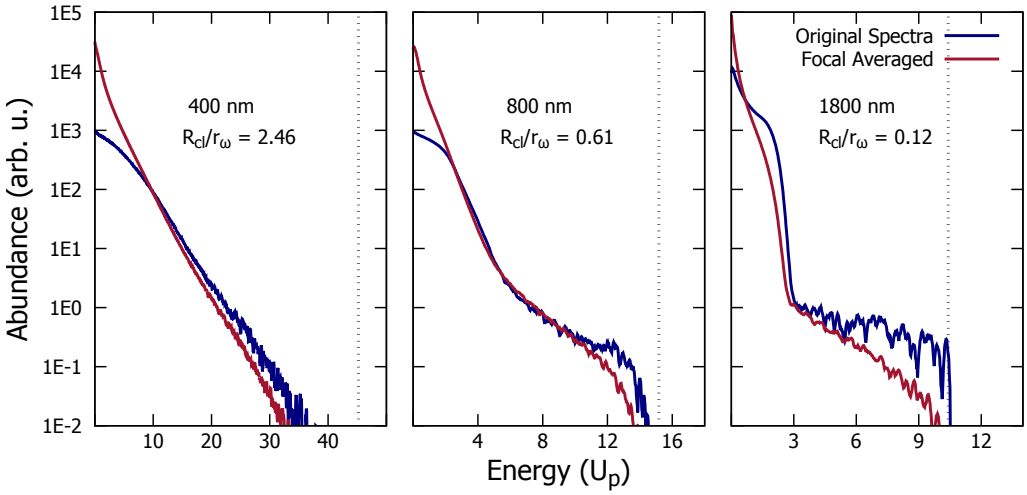

Figure S2: Examples of calculated focal averaged spectra (red lines) compared with the original single-intensity MD spectra (blue lines) used in its construction, for different values of wavelength and R. Vertical dashed lines indicate the energy of the fastest electron.

By solving the Hamiltons equations, we trace an outer-ionized electron from the nanocluster, starting at the right edge of the cluster at $x(t_0) = R_{\rm cl}$ with velocity $\dot{x}(t_0) = 0 \equiv p - A_0$ at a laser phase $\phi_0 = \omega t_0$. Within a full cycle of the laser pulse, the electron emerges from the cluster with final energy $E(\phi_0, x_r; R_{\rm cl}, V_{\rm cl})$ after an enforced elastic reflection of its momentum at some point $|x_r| \leq R_{\rm cl}$ within the cluster potential. To find the cutoff energy, this energy $E(\phi_0, x_r; R_{\rm cl}, V_{\rm cl})$ is maximized with respect to the initial phase ϕ_0 and x_r.

Defining $F_{\rm cl} = Q/R_{\rm cl}^2 = F_\omega$, the ionic potential can be scaled to the ponderomotive potential: $V_{\rm cl}/U_p \propto R_{\rm cl}/x_\omega$, making the Hamiltonian explicitly dependent only on the scaled cluster radius R (red line in Fig. S3). This scaling is essential to the universal dependence of the cutoff energy.

Limitations – Partial Charging: One of the main results of our model is that the production of energetic rescattered electrons benefits both from additional acceleration due to the cluster potential and the magnitude of the fields vector potential. These potentials however, develop and evolve in time. For the case of short laser pulses the energy gain process is affected in two ways; the cluster potential is not fully developed (i.e. does not fulfill the condition $Q = FR^2$) and the vector potential can vary significantly with respect to the pulse envelope (i.e. the carrier-envelope phase), therefore suppressing the energy gain.

The last return model can be readily modified to account for the effect of partial charging by means of a parameter β such that the total cluster charge is now given by $Q = \beta FR^2$. In this way short pulses with insufficient charging can be considered as the case where $\beta < 1$ while long pulses where cluster expansion and evaporation can occur correspond to cases with $\beta > 1$. The result from this modified scenario is shown in Fig. S3.

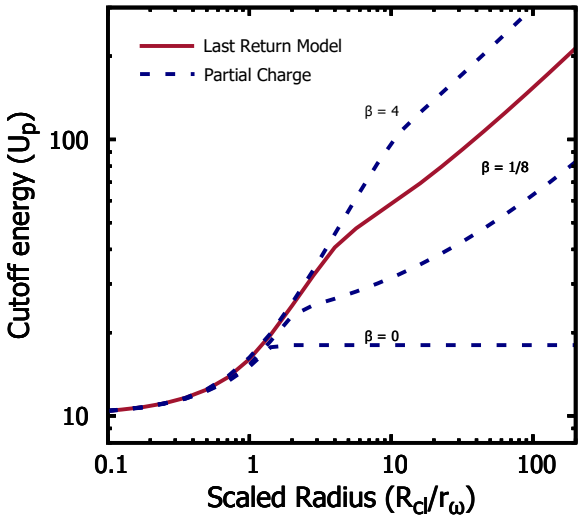

Figure S3: Modified last return model where the cluster charge is determined by the parameter β. For insufficient charging ($\beta < 1$) the energy gain is suppressed, while exceeding charge ($\beta > 1$) further enhances the electronic energies.

References

[S1] U. Even, EPJ Techniques and Instrumentation 2, 17 (2015).

[S2] O. F. Hagena, Rev. Sci. Instrum. 63, 2374 (1992).

[S3] D. W. Schumacher and P. H. Bucksbaum, Phys. Rev. A 54, 4271 (1996).

[S4] Y. L. Shao, T. Ditmire, J. W. G. Tisch, E. Springate, J. P. Marangos and M. H. R. Hutchinson, Phys. Rev. Lett., 77, 3343 (1996).

[S5] E. Springate, S. A. Aseyev, S. Zamith and M. J. J. Vrakking, Phys. Rev. A 68, 053201 (2003).

[S6] S. Alvarez, Dalton Trans. 42, 8617 (2013).